Space- and Time-Resolved Diffusion-Limited Binary Reaction Kinetics in Capillaries: Experimental Observation of Segregation, Anomalous Exponents, and Depletion Zone

Yong-Eun Lee Koo[1] and Raoul Kopelman[1]

An experimental investigation of one-dimensional, diffusion-limited $A + B \rightarrow C$ chemical reactions is reported. The persistence of reactant segregation and the formation of a depletion zone is observed and expressed in terms of the universal time exponents: α (motion of the boundary zone), β (width of instantaneous product formation zone), γ (rate of instantaneous local formation of product), δ (rate of instantaneous global formation of product), etc. There is good agreement with the recently predicted and/or simulated values: $\alpha = 1/2$, $\beta = 1/6$, $\gamma = 2/3$, $\delta = 1/2$, in contrast to classical predictions ($\alpha = 0, \beta = 1/2, \gamma = 0, \delta = -1/2$). Furthermore, classically the segregation would not be preserved and there would be no formation of a depletion zone and no motion (just dissipation) of the reaction zone. We also discuss the relations to electrode oxidation–reduction reactions, i.e., $A + C \rightarrow C$ where C is a catalyst, electrode, or "trap."

KEY WORDS: Reaction kinetics; diffusion; capillary; segregation.

1. INTRODUCTION

The Einstein–Smoluchowski approach to diffusion-limited reaction kinetics[1,2] is based on the following simple model. A mobile particle (walker) diffuses toward a fixed reactive particle (sitter). In the relevant diffusion equation the sitter acts as a "black hole." In spite of the historical anachronism regarding "black holes," this analogy was recognized and exploited by Chandrasekhar.[2] Moreover, he also described the diffusing

---

[1] Department of Chemistry, University of Michigan, Ann Arbor, Michigan 48109.
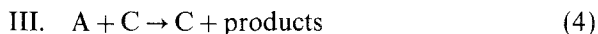
particle as a random walker, using a lattice model. Later, Montroll and Weiss[3] described analytically the space traced out by this walker as a function of time, i.e., the time dependence of the "average number of distinct sites visited" S. In three (and higher)-dimensional Euclidean space, S is linear in time (asymptotically), while in lower dimensions it is sublinear. The path (trace) of the random walker was shown by Mandelbrot[4] to be a fractal. Obviously the reaction occurs when this growing fractal path intersects with the "black hole." This was the basis for relating to S the probability of a particle being "trapped," in both Euclidean as well as non-Euclidean domains, such as percolation clusters.[5] Following Smoluchowski's heuristic generalization to many-particle systems, as well as the kinetic collision theory of gas reactions,[6,7] a similar generalization[8] was used to relate the reaction rate coefficient K to the trajectory (path) traced out per unit time. However, while K is time independent in both the collision theory of chemical kinetics and in Smoluchowski's approach (except for early times in the latter case), this is no longer true in our approach[5,8] (not even asymptotically) when S is sublinear in time. Thus, the rate coefficient $K(t)$ is no longer a "rate constant" and is given by[8,9]

$$K(t) \sim dS/dt \tag{1}$$

What are the implications of Eq. (1)? The rate coefficient K exemplifies the normalized instantaneous probability for the occurrence of reaction. It can easily be shown[10] that this probability is constant as long as the spatial distribution of particles is Poissonian. Maxwell hypothesized that all equilibrium distributions are Poissonian.[11] This resulted in a constant rate coefficient for binary collisions (rate $= K\rho^2$). In the collision theory of chemical reactions[6,7] it was implied that the above is still true even away from equilibrium. Practically this was justified because the fluid systems discussed were usually well-stirred mechanically or by convection. However, we assume below that the reaction occurs in a convectionless, nonstirred medium. We note that a reaction that is *not* reaction-limited may be "diffusion-limited" both in the presence and the absence of convection. The nonclassical, time-dependent rate coefficients occur only in the latter case, and even here mostly for low-dimensional reaction media (with some exotic exceptions[12-20]).

While it should be intuitively obvious that anomalous reaction rates imply non-Poissonian reactant distributions, this has not been realized until very recently (except for some exotic systems[14-20]). Specifically, a reactant may be surrounded by a *depletion zone* ("grey hole") *that grows in time* above and beyond what is expected from a Poissonian distribution. In short, there is a self-ordering of the reactants[21] that appears to be driven by a Darwinian-like "survival of the fittest" (or survival of the most isolated).

Specifically, non-Poissonian particle–particle distribution functions have been derived recently. The most amazing thing is the similarity among the distribution functions, and among the concomitant rate law anomalies, for different types of reactions. We discuss here briefly the three major types of elementary reactions (assumed to be irreversible):

$$\text{I.} \quad A + A \rightarrow \text{products} \tag{2}$$

$$\text{II.} \quad A + B \rightarrow \text{products} \tag{3}$$

$$\text{III.} \quad A + C \rightarrow C + \text{products} \tag{4}$$

where in cases II and III there is no hidden case I reaction (i.e., no $A + A$ or $B + B$ reaction).

The type I reaction [Eq. (2)] exhibits non-Poissonian (non-Hertz) nearest neighbor distance distributions in low-dimensional (including fractal) media.[10,21,22] The simplest case is given by one-dimensional media, where, in addition to approximate theories and computer simulation,[10,21,22] some exact analytical solutions have been derived.[23] Here the functional forms are essentially skewed-Gaussian or skewed-exponential, in contrast to the simple exponential (Poissonian) Hertz function.[2] On the other hand, in three-dimensional (Euclidean) space, the distribution is essentially Hertzian (Poissonian). The anomalous distributions are accompanied by anomalous rate laws. For instance,[10] for all one-dimensional type I cases (e.g., $A + A \rightarrow 0$ and $A + A \rightarrow A$),

$$\text{rate} = -d\rho/dt = k\rho^3 \tag{5}$$

which is equivalent *asymptotically* to

$$\text{rate} = K(t)\,\rho^2 \tag{6}$$

where $K(t)$ is given by Eq. (1), i.e.,

$$K(t) = k_0 t^{-1/2} \sim \rho(t) \tag{7}$$

because in one dimension $S \sim t^{1/2}$ and from Eqs. (5) and (6) it follows that $\rho \sim t^{-1/2}$.

Similar self-ordering is observed in steady-state situations (with input)[24] where the depletion zone and the characteristic time are related in analogy to Eq. (1).

For the type III reaction the situation is similar. For instance, in a one-dimensional medium with a single trap (or catalyst C) particle, exact analytical solutions[25] again give a skewed-Gaussian trap–walker distance distribution, accompanied by an anomalous rate law given by Eq. (1). The

situation for fractal and two-dimensional (Euclidean) media is similar.[26] Again, steady-state reactions (with input) show a similar behavior.[27]

Type II reactions are more complex, as the self-ordering may be macroscopic, i.e., leading to reactant segregation[15–20] and reaction surfaces.[28,29] However, the nearest-neighbor distance distributions show features similar to the other types.[22,30,31] For steady-state reactions, correlation lengths are again related to characteristic times in analogy to Eq. (1).[32] Of particular interest is the situation where streams of A and B reactants meet at a point or reaction front. This case was first analyzed by Galfi and Racz,[33] using an analytical formalism based on continuous reaction-diffusion equations. The validity of these results has been supported by random-walk Monte Carlo simulations in one and two dimensions[30,34,35] and more recently by a combination of analytical procedures and exact-enumeration random walk simulations.[36] What is special about this case is that it has been possible to observe experimentally not only the rate law, but also the segregation, the self-ordering, and, particularly, the reactant (and product interfaces) as function of time, quantitatively. Below we describe the experimental method as well as the resultant exponents and profile functions and their excellent agreement with both theory and simulations.

In Section 2 we give in detail the Galfi and Racz[33] model and its extensions.[34–36] The experimental setup and techniques are given in Section 3. Section 4 gives the experimental results and Section 5 the conclusions.

2. THEORETICAL MODELS

In the model of Galfi and Racz,[33] reactant A of constant density a_0 and B of constant density b_0 are initially separated. They meet at time 0, forming a single reaction boundary, which makes the system effectively one-dimensional. The motion of the reaction front with time is shown in Fig. 1. The results from the set of the reaction-diffusion equations for A and B, which are valid in the long-time limit, show that x_f (the position of the center of reaction front) scales with time as $x_f \sim t^{1/2}$, while w (the width of the reaction front) scales as $w \sim t^{1/6}$ and the production rate r_f (at $x = x_f$) scales as $t^{-2/3}$. Extrapolating their results,[33] we find[30,34] that the global reaction rate R scales as $t^{-1/2}$, i.e., $R = dC/dt \sim t^{-1/2}$.

Havlin et al. and Taitelbaum et al.[36] generalized this model in terms of the reacting species performing a random walk on a lattice, in which the rate at which the reaction A + B → products proceeds could be controlled. They compared this rate to the rate at which the steps were made to determine the width of the mixing layer (reaction front in Galfi and Racz
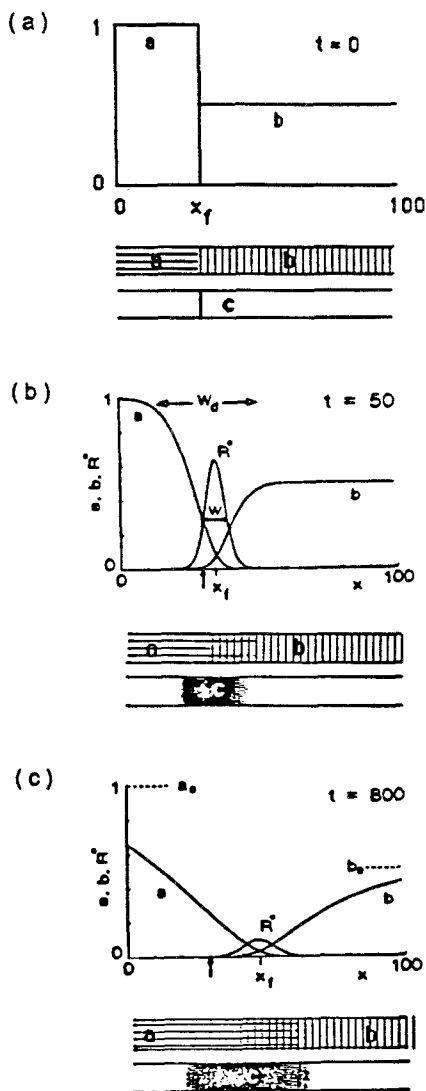
Fig. 1. The motion of the reaction front. Length (x), time (t), the densities (a, b) of the reagents (A, B), and the magnified production rate $(R^* = 100R = 100kab)$ of C are scaled to be all dimensionless. As an initial condition, we used $a = 1$, $b = 0$ for $x < 30$, and $a = 0$, $b = 0.5$ for $x > 30$ (the $t = 0$ position of the center of the front x_f is shown by an arrow). The top parts of (b) and (c) are from ref. 33.

description). They characterized the relation between reaction and diffusion as being diffusion-limited when the reaction time is negligible in comparison to the time of a single step of the random walk, and as being reaction-limited in the opposite case on which the classical kinetics is based. Using the exact enumeration method and analytical formalisms, they also found that the width of the mixing layer scaled as

$$W_{\text{int}} \sim n^{1/6} \tag{8}$$

for large n, where n is the number of steps (time) as predicted by the analytical study of Galfi and Racz. However, they also found that in the reaction-limited regime the width of the reaction front (or mixing layer) would be broader and scale as

$$W_{\text{int}} \sim n^{1/2} \qquad (\text{i.e., } t^{1/2}) \tag{9}$$

We expected[30] that the global reaction rate would increase as $t^{1/2}$ in the reaction-limited regime where the width of the reaction scales as $t^{1/2}$. Therefore, we must observe a crossover between the diffusion-limited regime and reaction-limited regime if the reaction rate is slow enough to show two regimes. Simulation as well as analytical results by Havlin *et al.* and Taitelbaum *et al.*[36] show such a crossover of the global reaction rate which lies between an increasing global reaction rate (at early time) and a decreasing such rate (after long time). In addition to the properties discussed by Galfi and Racz, Havlin *et al.* and Taitelbaum *et al.* also measured the nearest neighbor distance between A–B pairs for the diffusion-limited regime, which is

$$\langle L(n) \rangle_{nm} \sim n^{1/4}$$

Galfi and Racz's model is similar to that of Weiss *et al.*[25] for $A + C \rightarrow C$. In Weiss *et al.*'s model, an initially randomly distributed ensemble of Brownian particles (A) diffuses in a uniform field in the presence of a single trap C located at the origin in one dimension. Therefore, A is a one-dimensional continuous solute and C is a single trap in Weiss *et al.*'s model, while in Galfi and Racz's case, both A and B are continuous (and A and B are like traps to each other) and the system is not exactly one-dimensional, but is effectively one-dimensional, where the reaction-diffusion process occurs in three dimensions, but only the direction of the process is one-dimensional. The asymptotic global reaction rate of Weiss *et al.*'s was found to show the same time dependence as that derived[30] from the model of Galfi and Racz, i.e., decrease as $t^{-1/2}$: $dc_A/dt \sim t^{-1/2} c_A$. Weiss *et al.* also found the asymptotic time dependence of nearest-neighbor distances

between A–C pairs in one dimension, which go as $t^{1/4}$, the same time dependence as that of A–B pairs in Havlin *et al.*'s and Taitelbaum *et al.*'s result for Galfi and Racz's model.

Such similarity could also be found in a potential step electrochemical process under diffusion-limited conditions.[37] Let us assume that the electrode process involves an oxidized species O and a reduced species R, and that the process consists simply of the transfer of n electrons: $O + ne^- \leftrightarrow R$. Initially the solution is homogeneous and composed of species O only. The potential changes from the potential where no Faradaic process occurs, to the potential where the kinetics of the electron transfer at the electrode is so rapid that no reactant can coexist with the electrode. The electrode is planar, so that only diffusion along the x axis perpendicular to the electrode surface needs be considered. There are several mechanisms for transport of the ions or molecules to an electrode surface: diffusion, electric migration, and convection. The following precautions are taken to eliminate or reduce other transport mechanisms so as to have diffusion as the only mass transfer method: (1) The solution should not be stirred and the cell should be free of vibration. (2) The ratio of electrode area to solution volume should be small and experiments relatively short in duration so that relatively little electrolysis takes place, so as to minimize local changes in concentration or local heating which could lead to density gradients and convective mixing. (3) The solution should contain a large excess of an *inert electrolyte* to ensure that the electrical double layer is very compact and that the electric potential is nearly constant throughout the solution, thus minimizing electric migration effects.

Under such conditions, the resultant diffusion-limited current, which represents the global reaction rate, also shows a time dependence of $t^{-1/2}$, which is the same as that found for the model of Galfi and Racz. Experimentally, the oxidation of ferrocyanide ions using a suitable planar electrode under the conditions described above[38] was found to show the time dependence of $t^{-1/2}$.

This model can be referred to as $A + C \rightarrow C + B$ under the same effective one-dimensional conditions as those of Galfi and Racz's, where A is an oxidant (or reductant), B is a reductant (or oxidant), and C is the electrode. Alternatively, we can consider the electrode reaction in terms of a modified Galfi–Racz model, where A is the cation (anion) and B the electron (hole), but with a fixed boundary at the electrode–solution interface.

3. EXPERIMENTAL

3.1. Materials

Disodium ethyl bis(5-tetrazolylazo)acetate trihydrate (abbreviated "tetra" in this report) was synthesized and recrystallized as previous described.[39] Elementary analysis on the samples (which are recrystallized twice from alcohol) shows well-matched results with the calculated results based on the formula $C_8H_8O_2N_{12}Na_2 \cdot 3H_2O$ (Fig. 2) as shown below.

Calculated: C, 19.05%; H, 3.20%; N, 44.44%; Na, 12.16%.

Found: C, 18.86%; H, 3.11%; N, 43.65%; Na, 12.1%.

The absorption maxima for "tetra" in our work are also well matched with those of the literature values[39]: 270 and 410 nm. All the other chemicals used in this study were used as purchased. The copper(II) nitrate hydrate, 1.0 M bromine solution in carbon tetrachloride, cyclohexene, and the reagents for the synthesis of "tetra" were from Aldrich Chemical Co. and the agarose was from Sigma.

3.2. Reaction

We sought a proper reaction for this study which met the following requirements: (i) fast enough to ensure the diffusion-limited condition, (ii) one-to-one to be the bimolecular reaction, and (iii) the existence of suitable detection methods for the product and the reactants (especially reactions where the product and reactants show distinguishably different colors were preferred). Unfortunately, only a few reactions met such requirements and, furthermore, if a reaction is performed in a volatile organic solvent, the evaporation of the solvent ruins the experiments, since the diffusion process is very slow. Therefore, only reactions occurring in less-evaporable, viscous solvents are the proper choice. The following reactions were chosen: (1) bromine + cyclohexene → adduct in carbon tetrachloride and (2) Cu^{2+} + disodium ethyl bis(5-tetrazolylazo)acetate trihydrate ("tetra") → 1:1 complex in water. The reactants and product used in the
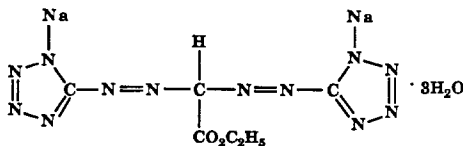

Fig. 2.   Structure of "tetra".

inorganic complex formation reaction are not so toxic compared to those in the organic addition reaction and it is easy to increase the viscosity of water by adding agarose. Therefore, the reaction $Cu^{2+} + $ "tetra" $\rightarrow 1:1$ complex was used for the experiments performed using an automatic computerized setup, although both reactions were tested successfully in the preliminary experiments shown in Section 4.1.

3.3. Apparatus

The early preliminary experiments were performed using a glass reactor (Fig. 3), ruler or metric paper, and stopwatch. Later, a sophisticated and computerized experimental setup was used for monitoring the absorbance of the reactant and product as shown in Figs. 4A and 4B. The on/off of the lamp and solenoid were controlled through the parallel port of the computer and the movement of the stepping motor (from New England Affiliated Technologies, Inc.) was controlled through the RS232 port of the computer via a stepping motor controller (from Techno). Mechanical resolution for the motor was 0.1 mm throughout the experiments. The light source, solenoid with two filters, slit unit, and detector were fixed on the stepping motor and a glass reactor was fixed over the slit unit separately from all other units. The detector is connected to the A/D board of the computer to digitize the analogue data and store them in the computer. Two small fans were used to cool down the stepping motor controller and the power source for the lamp and solenoid. Details about each unit of the computerised automatic setup are described below.

3.3.1. Reactor. The reactors used for measurements of diffusion coefficients in the 1930s and 1940s were all vertical reactors which used gravity to make the boundary flat.[40–43] However, we used the horizontal reactor to get rid of such a "dirty" trick: a glass reactor made of square or rectangular tube (2×2 mm or 4×2 m I.D.) with a small center hole, which is specially made using a special drill or a hot tungsten rod rather than using a typical glass-blowing technique, so as not to change the inside surface of the reactor, and used as an air outlet (Fig. 3).
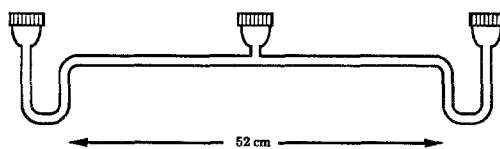

Fig. 3.   Glass reactor.

3.3.2. Light Source. According to absorption spectra (Fig. 5), the best wavelength for the inorganic product excitation was 535 nm and that for the reactant excitation was 410 nm. We initially used a green LED (4308H5 from IDI, 565 ± 14 nm) which could be used for monitoring the product only, and thus, later, a halogen lamp (HPR50 from Radio Shack) with two bandpass filters, 540 ± 10 nm for product and 415 ± 8 nm for reactant "tetra", was used.

3.3.3. Detector and Noise Reduction. We used a PMT (R446HA from Hamamatsu) in PMT housing (from Pacific Instruments)
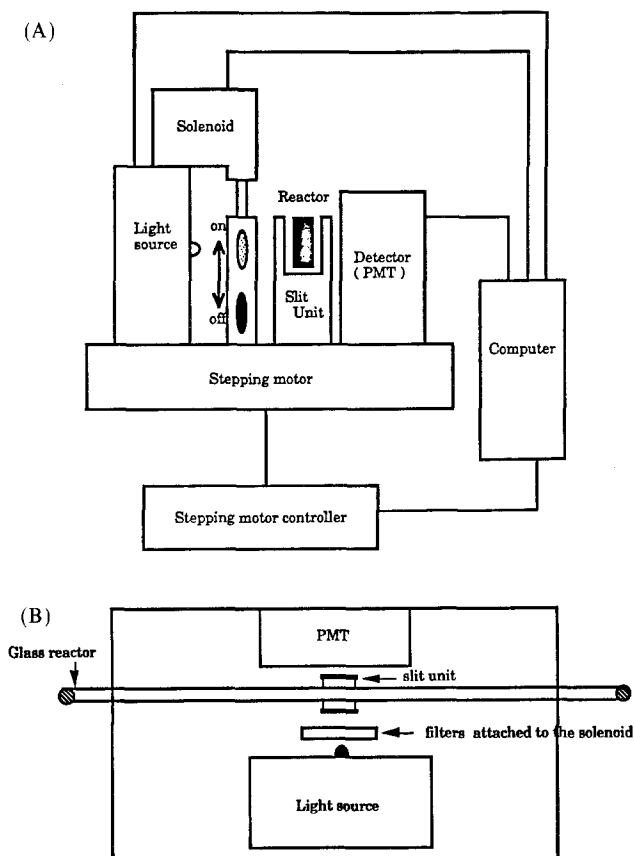

Fig. 4. (A) Schematic diagram for the experimental setup for the absorbance measurement along the reaction front domain. (B) Top view of the experimental setup for the absorbance measurement.
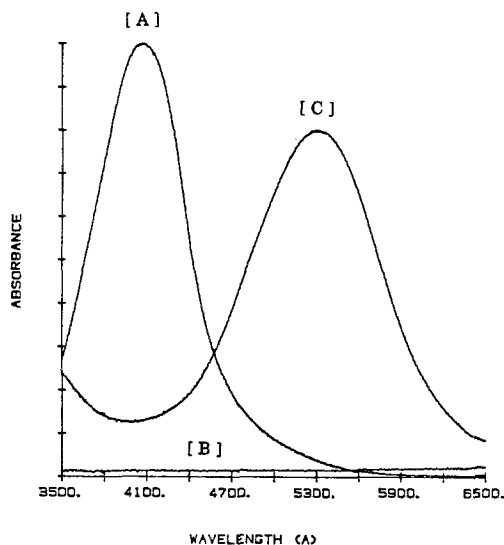
Fig. 5. The absorption spectra of reactant copper ion [B], "tetra" [A], and the product (Cu^{2+}–"tetra" complex). Concentration of the copper ion was 2×10^{-3} M, that for the "tetra" was 6×10^{-5} M, and that for the product was also 6×10^{-5} M.

for a detector. The digitized output of PMT through the A/D board contains a lot of noise. For noise reduction, we added a low-pass filter (using 0.01-mF and 1-M resistor) and averaged the signal at each data point. By using the low-pass filter, the noise is reduced by five times, but it becomes slower to respond because of a longer rising time to reach the new voltage. The actual rising time of the low-pass filter was 25 msec. Due to such a slow response, we put a delay time of 35 msec before the PMT reads the signal, which in return slowed down the scanning rate aong the reaction front domain, i.e., it takes about 35 sec to scan 6 cm using 0.1 mm mechanical resolution. However, such scanning is still effectively the same as taking snapshots of the reaction front domain, since it takes more than 2 min to move 0.1 mm even in the first scan (after 10 min) when the average moving distance is the largest.

3.3.4. Slit Unit. The slit unit was composed of two slits which were well aligned (Fig. 6). Each slit was made of a hole of size 4×1.8 mm and two movable matching stainless steel blades which covered the hole. We used the slit width of 0.05 mm on the light source side and 0.09 mm on the detector side to ensure a 0.1 mm mechanical resolution.
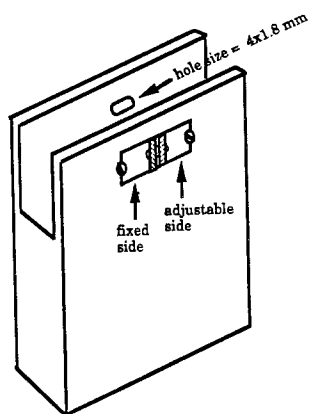
Fig. 6. Slit unit: the slit unit is composed of two slits, the width of which is adjustable. For the present experiments, the slit width of 0.05 mm was used for the light source side and that of 0.09 mm was used for the detector side.

3.4. Procedure

After a few minutes degassing of each of the reactant solutions in an ultrasonic cleanser to get rid of air bubbles, the two reactants were poured into each end arm of the glass reactor slowly by using syringes. They met at the center, forming a vertical boundary where the product was being formed, at time 0. The first scan along the reaction front domain starts after 10 min. The time interval between scans was initially 10 min and it was slowly increased up to 100 min. The lamp was "on" 4 min before each scanning, and the solenoid was "on or off" (i.e., to move upward or downward to choose a suitable filter) 30 sec before scanning. When the solenoid was on, the top filter was used and when it was off, the bottom filter was used. (When a green LED was used for a light source, it was on all the time because it had a longer lifetime and produced no heat.) The scanning process is composed of the following steps: (i) move in steps corresponding to the experimental resolution (0.1 mm in this experiment); (ii) take many data (up to 99) at a fixed point and send them to the A/D board and average them; (iii) repeat (i) and (ii) until the stepping motor reaches the end of the reaction front domain. Since the light source, solenoid, sli unit, and detector are fixed on the stepping motor, they are moving simultaneously with the stepping motor along the whole reaction front domain, the length of which is less than 5 cm after 24 hr.

After scanning, the data were automatically stored and the lamp and solenoid were turned off and the stepping motor was moved back to its original position and stayed there until the next scan started. The specific

computer programs for such mechanical control, data collection, and
further data analysis were written in Turbo Pascal language. A functionally
similar absorbance scanning device was built by Minton *et al.* using a com-
mercial UV-US spectrophotometer.[44] However, their device is inadquate
for our purpose, since the direction of scanning is vertical.

4. RESULTS AND DISCUSSIONS

4.1. Preliminary Experiments

In order to seek a proper realization for the bimolecular reaction
$A + B \rightarrow C$ and a proper reactor, the motions of the reaction boundaries
were followed for several reactions performed in different reactors using a
ruler or metric paper and a stopwatch. The reactions and the reactor were
chosen as described in Sections 3.2 and 3.3. Preliminary results from such
measurements are summarized in Table I. Using a gel as a solvent for the
inorganic reaction resulted in the boundary being vertical even in a
relatively big 4×2 mm tube and also prevented convection, but allowed
efficient diffusion. Although the obtained preliminary time exponents α (for
boundary motion) for all cases shown in Table I were well matched with
the theoretical value $1/2$, the inorganic bimolecular complex formation
reaction [Cu^{2+} + disodium ethyl bis(5-tetrazolylazo)acetate trihydrate
("tetra") → 1:1 complex in a gel] performed in the rectangular or square
glass reactor was chosen due to the following reasons: (1) The reaction was
instantaneous and we could easily monitor simultaneously both one

Table I.   Results from Preliminary Experiments[a]

	α	Reactor
Reaction		
2.4 M $C_6H_{10} + 10^{-1}$ M Br_2	0.47	Round capillary I.D. = 1/4–3/4 mm
1.5×10^{-4} M $Cu^{2+} + 10^{-3}$ M "tetra"	0.56	Rectangular tube I.D. = 4 × 2 mm
1.5×10^{-4} M $Cu^{2+} + 10^{-3}$ M "tetra"	0.55	Square tube I.D. = 2 × 2 mm
Diffusion only		
5×10^{-4} M Sulfonazo III in		
agar/water	0.57	Round capillary I.D. = 1/4–3/4 mm
10^{-4} M Cu^{2+}–"tetra" complex		
in agarose/water	0.48	Rectangular tube I.D. = 4 × 2 mm
2×10^{-4} M Cu^{2+}–"tetra"		
complex in agarose/water	0.59	Square tube I.D. = 2 × 2 mm

[a] α is the time exponent for the movement of the reaction front, i.e., $x_f \sim t^\alpha$.

reactant and one product through optical absorbance measurements. (2) The rectangular or square tubes are better than the round capillary for the spectroscopic measurement.

To choose a suitable concentration of the aqueous agarose solution for a gel, the concentrations of 0.1–0.5% were tested: At 0.1%, we could not achieve a vertical boundary. As the concentration became higher, the viscosity and the turbidity of the solution and also the risk of air bubbles bigger. The lowest concentration to give a vertical boundary, 0.15%, was chosen. The viscosity of the 0.15% aqueous agarose solution was found to be 11 times greater than that of water. The relative viscosity (to pure water) of other concentrations are as follows: 13 for 0.2%, 73 for 0.4%, and 96 for 0.5%.

Another observation from this preliminary experiment was that the boundaries formed in the reaction process were considerably sharper than those in the reactionless diffusion process, indicating that $\beta \ll \alpha = 1/2$.

4.2. Results from Optical Absorbance Measurements

4.2.1. Time Exponents.
The observed reaction was Cu^{2+} + "tetra" → 1:1 complex in an 0.15% agarose/water solution. The absorption maxima of the reactant "tetra" and the product are well separated and the copper absorbance is negligible (see Fig. 5) and both the reactant "tetra"
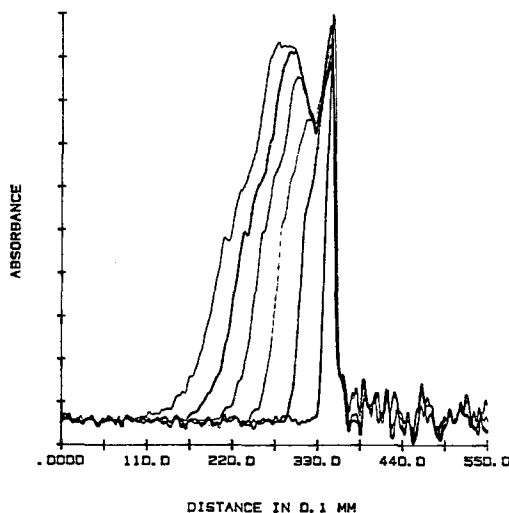

Fig. 7. The absorbance of the total accumulated product in the reaction of 6×10^{-5} M "tetra" + 2×10^{-3} M Cu^{2+}: from the right, $t = 10, 56, 160, 314, 518, 772$ min. (light source: halogen lamp, 4×2 mm glass reactor).

and the product obey the Beer–Lambert law under experimental conditions (up to 2×10^{-4} M). The optical absorbance of the total accumulated product was measured along the reaction front domain at fixed time intervals (initially 10 min and slowly increased up to 100 min) as shown in Fig. 7. From the differences of such absorbances of the total product measured at consecutive times, we could find the product formation per unit time at each moment (see Fig. 8), where we could see the movement of the center of the reaction front toward the minority reactant side (in this case, the minority reactant was in the left side), as well as the decrease of the production rate and the slow increase in the width of the reaction front. Inside the reaction front domain, the concentration of the two reactants was very low due to the product formation. Therefore, the reaction front actually formed a gap between the two reactants and such a gap opening became bigger as the width of the reaction increased with time, which kept the two reactants segregated throughout the experiments.

The width of the reaction front and the position of the center of the reaction front were measured at each moment. The global reaction rate was calculated from the subtraction of the total accumulated production area calculated at consecutive times (Fig. 7) rather than the area from already subtracted profiles (Fig. 8) to reduce the errors. The time exponent for each case was obtained from the log–log plot as shown in Figs. 9A–9C. We
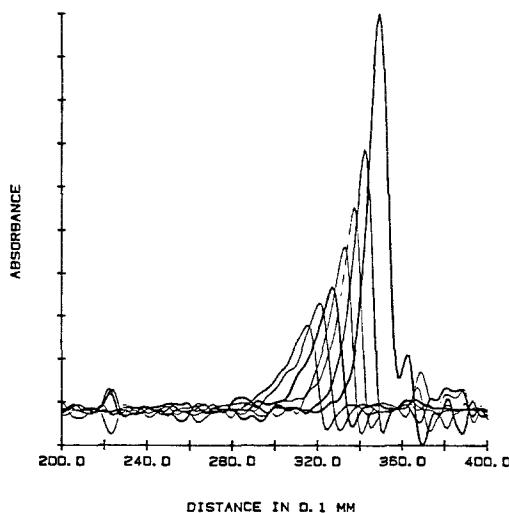

Fig. 8. The absorbance of the product formation per unit time at the reaction front in the reaction of 6×10^{-5} M "tetra" $+ 2 \times 10^{-3}$ M Cu^{2+}: from the right, $t = 16$, 27, 39, 51, 67, 88, 109 min (light source: halogen lamp, 4×2 mm glass reactor).
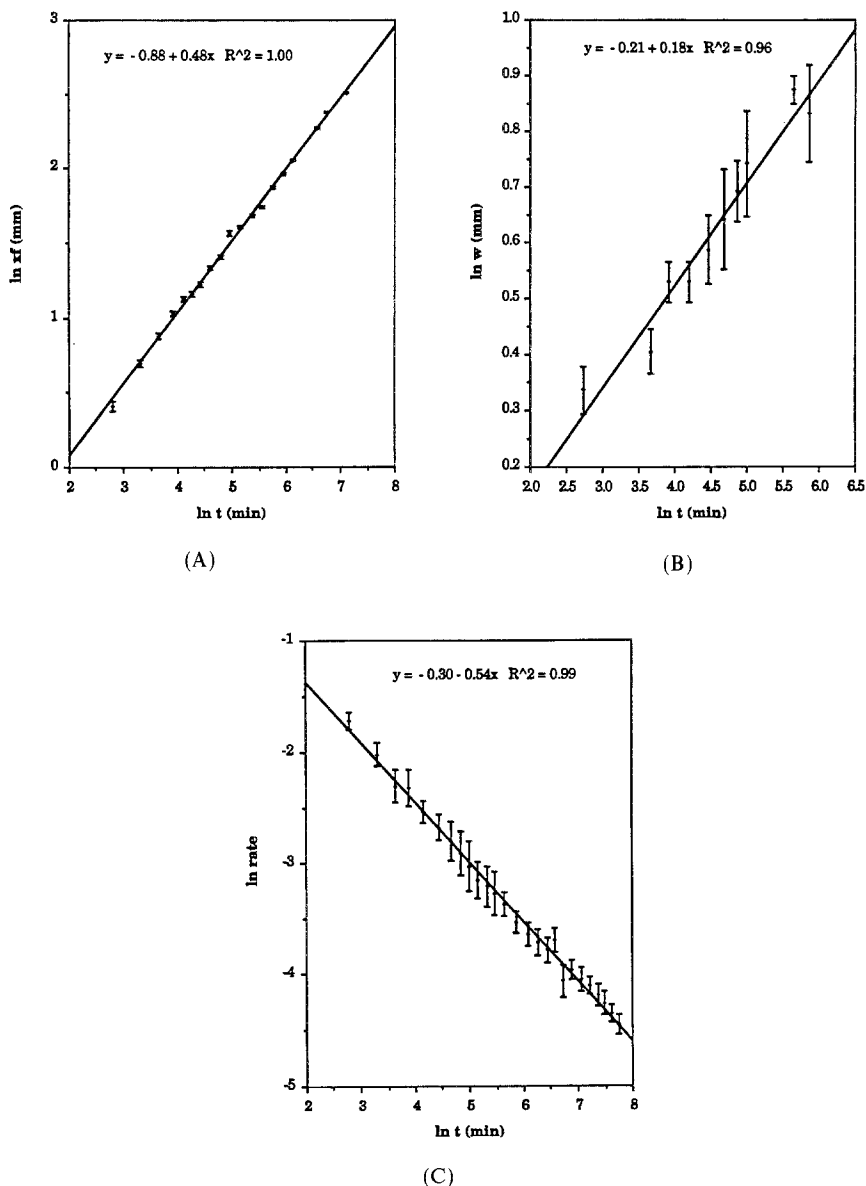
(A)

(B)

(C)

Fig. 9.   (A) Plot of log x_f vs. log t in the reaction of 5×10^{-5} M "tetra" $+ 10^{-3}$ M Cu^{2+}, giving $\alpha = 0.48 \pm 0.04$ (light source: green LED, 4×2 mm glass reactor). (B) Plot of log w vs. log t in the reaction of 6×10^{-5} M "tetra" $+ 2 \times 10^{-3}$ M Cu^{2+}, giving $\beta = 0.18 \pm 0.04$ (light source: halogen lamp, 4×2 mm glass reactor). (C) Plot of log global rate vs. log t in the reaction of 7.5×10^{-5} M "tetra" $+ 10^{-3}$ M Cu^{2+}, giving $\delta = 0.54 \pm 0.05$ (light source: green LED, 4×2 mm glass reactor).

Table II. Time Exponents from Experiment[a]

Reactor size	C_{Cu}	C_{tetra}	α	β	δ
4×2 mm	10^{-3} M	5×10^{-5} M	0.48, 0.54	0.17, 0.15	0.53, 0.55
	10^{-3} M	7.5×10^{-5} M	0.53, 0.49	0.15, 0.20	0.51, 0.54
	2×10^{-3} M	6×10^{-5} M	0.52, 0.50	0.16, 0.18	0.52, 0.55
2×2 mm	2×10^{-3} M	6×10^{-5} M	0.60	0.22	0.52

[a] C_{Cu} and C_{tetra} are the $t = 0$ concentrations for Cu^{2+} and "tetra", respectively. "Tetra" is disodium ethyl bis(5-tetrazolylazo)acetate trihydrate, where the solvent is 0.15% agarose/water. Here, $x_f \sim t^{\alpha}$, $w \sim t^{\beta}$, and $R \sim t^{-\delta}$. The values of α, β, δ were measured twice for the 4×2 mm reactor.

could notice that experimental data of the global reaction rate do not show any indication of the increasing early stage, but only a decreasing trend as $t^{-1/2}$, which indicates that the present observed system is totally in the diffusion-limited regime. The error bars for the width and the position of the reaction front were from direct measurements and that for the global reaction rate from the calculations[45],2 based on the standard deviations of the baseline of the two consecutive total production profiles. All the time exponents obtained are collected in Table II. These results agreed well with the theoretical expectations[33,36] and simulation results[30,34] as shown in Table III.

4.2.2. Experimental Reactant Profiles.

The profiles of the reactant "tetra" were monitored in three different cases as shown in Figs. 10–12: (1) in the reaction-diffusion process, where it existed as a minority reactant; (2) in the reaction-diffusion process, where it existed as a majority reactant; (3) in the diffusion-only process. The profiles of the

Table III. Comparison of Time Exponents[a]

	α	β	γ	δ	ε
Experiment	0.51 ± 0.03	0.17 ± 0.03	0.70^b	0.53 ± 0.02	0.45 ± 0.01
Simulation	0.52 ± 0.03	0.16 ± 0.01	0.68^b	0.52 ± 0.02	—
Theory	1/2	1/6	2/3	1/2	1/2

[a] Here $x_f \sim t^{\alpha}$, $w \sim t^{\beta}$, $r_f \sim t^{-\gamma}$, $R \sim t^{-\delta}$, and $\bar{x}$ (average distance from the origin) $\sim t^{\varepsilon}$. The theoretical values of α, β, γ, and δ are from refs. 30 and 33 and that of ε is from Einstein's diffusion theory (see refs. 1 and 2).

[b] Difficult to measure experimentally and in the simulation, but derived from the theoretical relation[30,33] $\gamma = \beta + \delta$.
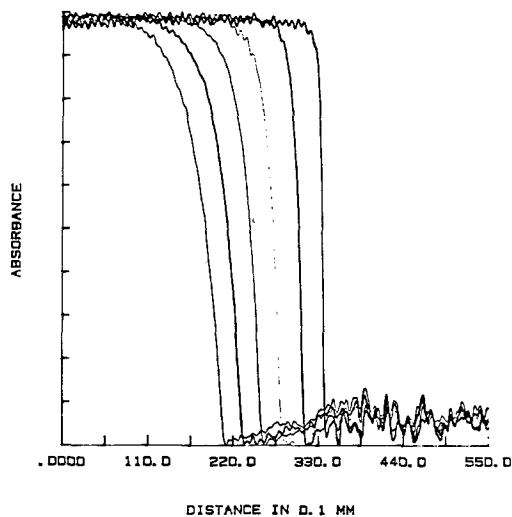
Fig. 10. Absorvance profiles of the reactant "tetra" when it existed as the minority compo-
nent in the reaction: from the right, $t = 11$, 58, 161, 315, 519, 774 min in the reaction of
6×10^{-5} M "tetra" $+ 2 \times 10^{-3}$ M Cu^{2+} (light source: halogen lamp, 4×2 mm glass reactor).
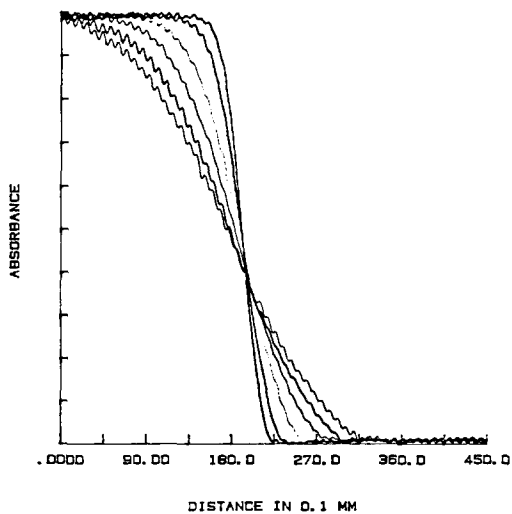

Fig. 11. Absorbance profiles of the reactant "tetra" when it existed as the majority in the
reaction: moving to the right (bottom), $t = 22$, 57, 161, 316, 521, 776 min in the reaction of
10^{-4} M "tetra" $+ 10^{-5}$ M Cu^{2+} (light source: halogen lamp, 4×2 mm glass reactor).
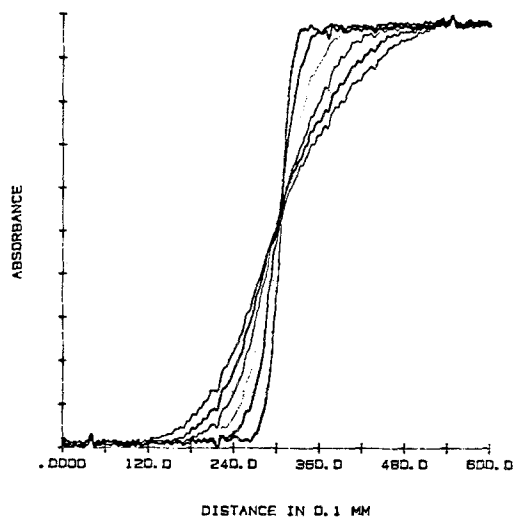
DISTANCE IN 0.1 MM

Fig. 12. Absorbance profiles of the reactant "tetra" in the diffusion-only process: moving to the left (bottom), $t = 11$, 56, 158, 310, 513, 766 min in the diffusion of 6×10^{-5} M "tetra" (light source: halogen lamp, 4×2 mm glass reactor).
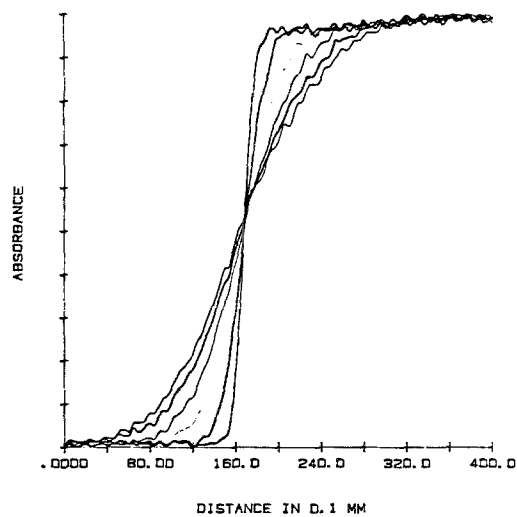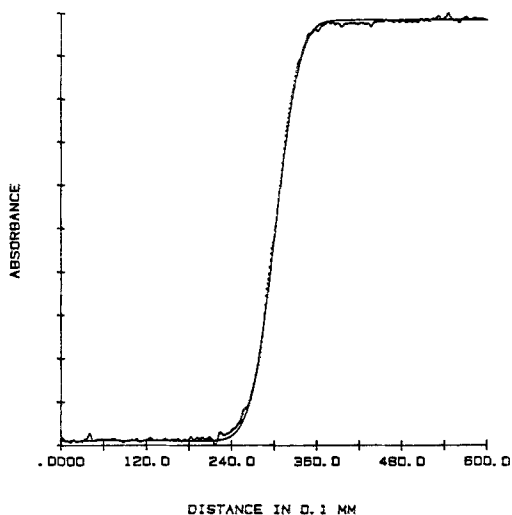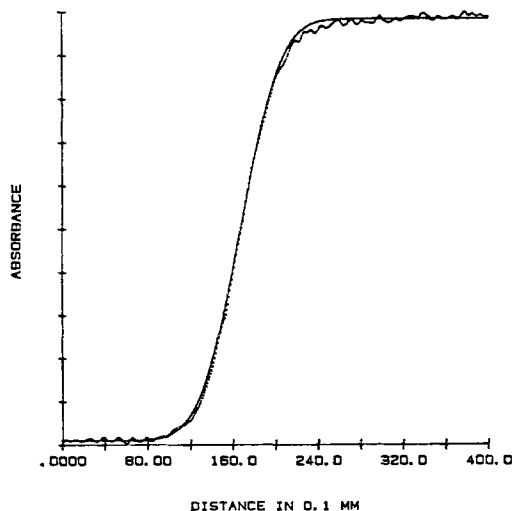

DISTANCE IN 0.1 MM

Fig. 13. Absorbance profiles of the product in the diffusion-only process: moving to the left (bottom), $t = 10$, 52, 156, 326, 514, 741 min for the diffusion of 10^{-4} M product (light source: green LED, 4×2 mm glass reactor).
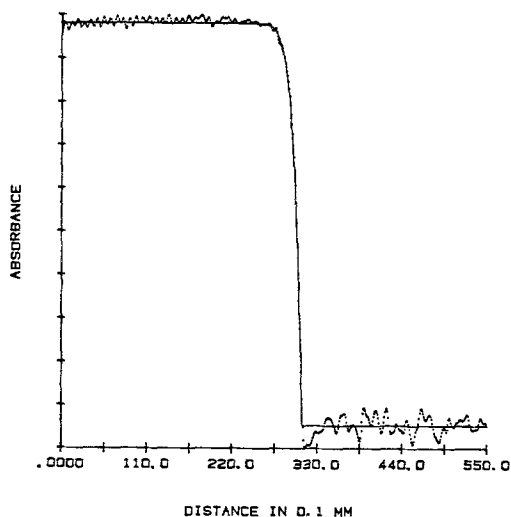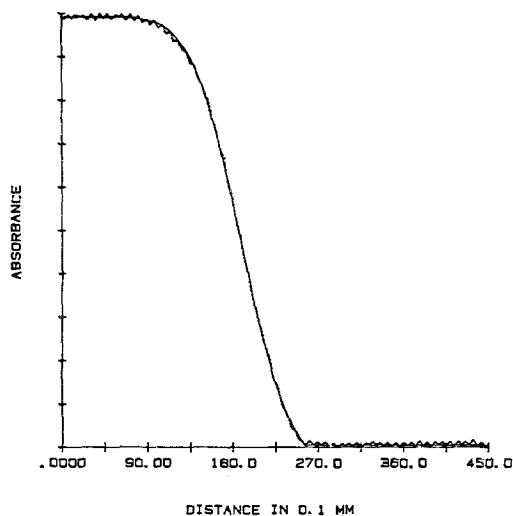
(A)

(B)

Fig. 14. (A) The profile of "tetra" in the diffusion-only process: initial concentration of "tetra" $= 6 \times 10^{-5}$ M, $t = 56$ min. The dotted line indicates the experimental curve and the solid line indicates the fitted curve (light source: halogen lamp, 4×2 mm glass reactor). (B) The profile of the product in the diffusion-only process: initial concentration of product $= 10^{-4}$ M, $t = 156$ min. The dotted indicates the experimental curve and the solid line indicates the fitted curve (light souce: green LED, 4×2 mm glass reactor).

(C)

(D)

Fig. 14. (*Continued*) (C) The profile of "tetra" as the minority in the reaction of 6×10^{-5} M "tetra" $+ 2 \times 10^{-3}$ M Cu^{2+}, $t = 58$ min. The dotted line indicates the experimental curve and the solid line indicates the fitted curve (light source: halogen lamp, 4×2 mm glass reactor). (D) The profile of "tetra" as the majority in the reaction of 10^{-4} M "tetra" $+ 10^{-5}$ M Cu^{2+}, $t = 161$ min. The dotted line indicates the experimental curve and the solid line indicates the fitted curve (light source: halogen lamp, 4×2 mm glass reactor).

product for the diffusion-only process were also monitored for comparison purposes (Fig. 13). The profiles of both minority and majority "tetra" in the reaction processes (Figs. 10 and 11) showed the movement of the "cutting point" where the concentration of "tetra" was 0, due to the reaction with the other reactant (copper ion), which implied the movement of the reaction front, although the minority case showed such an effect more drastically. All profiles for the majority reactant met at one point and seemed to be the same as that for the pure diffusion process, except that a part of its profile was consumed by the minority reactant.

We measured the time dependence of the "average moving distance" for the diffusion of "tetra" in the reaction case, when it was the majority component, and also in the diffusion-only process: The time exponent for the diffusion-only process was 0.46, which is close to 0.5, the predicted value by Einstein's law. For the majority reactant in the reaction case, it was 0.45, which supported the fact that the diffusion of the reactant during the reaction-diffusion process was the same as that for the pure diffusion process. This time exponent was predicted theoretically by Havlin et al.[36]

4.2.3. Curve Fitting for the Reactant Profiles

4.2.3.1. For the Diffusion-Only Process. The simple diffusion of a reactant under the present experimental conditions can be described by Fick's second law with initial boundary conditions:

$$\text{for } t = 0, \qquad c(x, 0) = 0 \qquad \text{for } x < 0 \tag{10a}$$

$$c(x, 0) = c_0 \qquad \text{for } x > 0 \tag{10b}$$

where c_0 is the initial concentration of the reactant and D is the diffusion coefficient.

Assuming that during the diffusion process no concentration changes occur at the extreme ends of the reactor, we obtain the following relation between c, x, and t, which was used for the fitting[41]:

$$c_x = (c_0/2) \left[1 - 2/\sqrt{\pi} \int_0^y \exp(-y^2) \, dy \right], \qquad \text{where } y^2 = x^2/4Dt \tag{11}$$

Since both the concentration vs. distance profiles (actually, optical absorbance in our case) and the time for each profile were measured from the experiments, the diffusion coefficient was the only parameter for the fitting.

4.2.3.2. For the Reaction-Diffusion Process. We assumed that the diffusion of the reactant for both the majority case and the minority case was the same as that for the diffusion process, although part of the reactant

disappeared due to the reaction process. Therefore, the fitting equation for the reaction case is basically the same as that for a simple diffusion case, except that we set the y value of the cutting point as 0:

$$c_{cop} = (c_0/2) \left[1 - 2/\sqrt{\pi} \int_0^{y_{cop}} \exp(-y^2) \, dy \right] \tag{12}$$

$$c_x = c^* \left\{ (c_0/2) \left[1 - 2/\sqrt{\pi} \int_0^y \exp(-y^2) \, dy \right] - c_{cop} \right\} \tag{13}$$

where c_{cop} is the calculated concentration of the cutting point based on the pure diffusion-only case and c^* is the calculated constant to make $c_\infty = c_0$.

Since the position of cop (cutting point) and c^* were obtained from experiments, the diffusion coefficient was the only parameter for fitting in this case, too.

The fitting curves are well matched with the experimental results, as can be seen in Figs. 14A–14D. The resulting diffusion coefficients for each case are summarized in Table IV. As can be seen, the diffusion coefficients for "tetra" $[(8.0 \pm 0.5) \times 10^{-10}$, $(8.7 \pm 0.3) \times 10^{-10}$, $(8.8 \pm 0.3) \times 10^{-10}$ m^2/sec] are almost the same for all three cases, proving that the diffusion is almost left intact by the reaction. The diffusion coefficient for the product was found to be about half of that of "tetra" $[(4.6 \pm 0.3) \times 10^{-10}$ m^2/sec].

Using the same fitting methods, we also measured the diffusion coefficients of the "tetra" in 0.2% and 0.4% agarose solution in addition to that of "tetra" in 0.15% agarose solution, by running the diffusion-only process to test the efficiency of the diffusion in highly viscous solutions.

The measured diffusion coefficients are shown in Table V together with corresponding viscosities. The viscosities of the aqueous agarose solution were measured by using the Ubbelohde viscometer.[46] We note that the diffusion coefficient of the 0.4% agarose solution does not change much (only 20% decrease) from that of the 0.2% agrose solution although the

Table IV. Diffusion Coefficients for "Tetra" from Fittings[a]

Case	Best fitting D (m^2/sec)
Minority diffusion in reaction	$(8.0 \pm 0.5) \times 10^{-10}$
Majority diffusion in reaction	$(8.7 \pm 0.3) \times 10^{-10}$
Diffusion-only process	$(8.8 \pm 0.3) \times 10^{-10}$

[a]Best fitting D for the product was $(4.6 \pm 0.3) \times 10^{-10}$ m^2/sec (in 0.15% agarose solution).

Table V.   Diffusion Coefficients and the Viscosities of "Tetra" from Diffusion-Only Process

Percent of agarose solution	0.15	0.2	0.4
Relative viscosity to water	11	13	73
D (m^2/sec)	8.8×10^{-10}	7.4×10^{-10}	5.9×10^{-10}

viscosity of the 0.4% solution increased abruptly from that of the 0.2% solution (factor of 6), which means that the diffusion is still effective in highly viscous solutions.

5. CONCLUSIONS

Self-ordering and segregation effects in diffusion-limited $A + B \rightarrow$ products reactions have been indicated by theories and simulations and have drawn much interest, but have lacked experimental evidence. The work presented in this paper is the first experimental study to show the existence and persistence of reaction segregation effects for elementary bimolecular reactions, for the case predicted in the theoretical work of Galfi and Racz.

The diffusion-controlled chemical reaction $A + B \rightarrow$ products was studied under initially segregated conditions using an instantaneous complex formation reaction, and the segregation of the reactants in time and the time dependence of the properties of the reaction front were investigated. In contrast to the classical expectation (reaction-limited regime), the two reactants do not interdiffuse, but a reactant gap opens up, in this case of an initially segregated situation. Inside the gap the concentrations of A and B are very low. They decrease in time even as the gap increases in time. Therefore the initial segregation is maintained throughout the reaction. This creation of a depletion zone causes the reaction rate to decrease in time as $t^{-1/2}$ while the reaction rate in the reaction-limited regime is supposed to increase with time as $t^{1/2}$.

The experimental time exponents (the position of the center of the reaction front, the width of the reaction front, and the global reaction rate of the reaction front) are in quantitative agreement with both the simulations and the theory, as shown in Table III. The reactant profiles were monitored both during the reaction and the diffusion-only process and analyzed by a curve-fitting process. All the reactant profiles fit well the simple diffusion profiles from Fick's second law and also exhibit almost the same diffusion coefficients, irrespective of the existence of reaction, which

indicates that the diffusion process is almost left intact during the reaction. In addition, the diffusion coefficients are found not to depend much on the viscosities.

ACKNOWLEDGMENTS

REFERENCES

1. M. V. Smoluchowski, *Z. Phys. Chem.* **92**:129 (1917).
2. S. Chandrasekhar, *Rev. Mod. Phys.* **15**:1 (1943).
3. E. W. Montroll and G. W. Weiss, *J. Math. Phys.* **6**:167 (1965).
4. B. B. Mandelbrot, *Fractals: Form, Change and Dimension* (Freeman, San Francisco, 1977); *The Fractal Geometry of Nature* (Freeman, San Francisco, 1983).
5. J. Hoshen and R. Kopelman, *J. Chem. Phys.* **65**:2817 (1976).
6. W. J. Moore, *Physical Chemistry*, 4th ed. (Prentice-Hall, Englewood Cliffs, New Jersey, 1972).
7. W. C. McLewis, *J. Chem. Soc.* **113**:471 (1918).
8. P. Argyrakis and R. Kopelman, *J. Chem. Phys.* **72**:3053 (1980).
9. P. Argyrakis and R. Kopelman, *Chem. Phys. Lett.* **61**:187 (1979).
10. R. Kopelman, *Science* **241**:1620 (1988).
11. R. Feynman, R. B. Leighton, and M. Sands, *The Feynman Lectures on Physics*, Vol. 1 (Addison-Wesley, Reading, Massachusetts, 1963).
12. B. Ya. Balagurov and V. G. Vaks, *Zh. Eksp. Teor. Fiz.* **65**:1939 (1973) [*Sov. Phys.-JETP* **38**:968 (1974)].
13. M. D. Donsker and J. R. S. Varadhan, *Commun. Pure Appl. Math.* **28**:525 (1975).
14. V. M. Agranovich and M. D. Galanin, *Electronic Excitation Energy Transfer in Condensed Matter* (North-Holland, Amsterdam, 1982).
15. A. A. Ovchinikov and Ya. B. Zeldovich, *Chem. Phys.* **28**:215 (1978).
16. D. Toussaint and F. Wilczek, *J. Chem. Phys.* **78**:2642 (1983).
17. K. Kang and S. Redner, *Phys. Rev. Lett.* **52**:955 (1984).
18. G. Zumofen, A. Blumen, and J. Klafter, *J. Chem. Phys.* **83**:3198 (1985).
19. K. Lindenberg, B. J. West, and R. Kopelman, *Phys. Rev. Lett.* **60**:1777 (1988).
20. K. Lindenberg, B. J. West, and R. Kopelman, *Phys. Rev. A* **42**:890 (1990).
21. R. Kopelman, S. J. Parus, and J. Prasad, *Chem. Phys.* **128**:209 (1988).
22. P. Argyrakis and R. Kopelman, *Phys. Rev. A* **41**:2114, 2121 (1990).
23. C. R. Doering and D. Ben-Avraham, *Phys. Rev. A* **38**:3035 (1988); D. Ben-Avraham and C. R. Doering, *Phys. Rev. Lett.* **62**:2563 (1989).
24. E. Clement, L. M. Sander, and R. Kopelman, *Phys. Rev. A* **39**:6472 (1989).
25. G. Weiss, R. Kopelman, and S. Havlin, *Phys. Rev. A* **39**:466 (1989); H. Taitelbaum, R. Kopelman, G. H. Weiss, and S. Havlin, *Phys. Rev. A* **41**:3116 (1990).

26. S. Havlin, H. Lattralde, R. Kopelman, and G. H. Weiss, *Physica A* **169**:337 (1990); R. Schoonover, D. Ben-Avraham, S. Havlin, R. Kopelman, and G. H. Weiss, *Physica A* **171**:232 (1991).
27. E. Clement, R. Kopelman, and L. M. Sander, *Europhys. Lett.* **11**:707 (1990).
28. W.-S. Sheu, K. Lindenberg, and R. Kopelman, *Phys. Rev. A* **42**:2279 (1990).
29. K. Lindenberg, W.-S. Sheu, and R. Kopelman, *Phys. Rev. A*, in press.
30. L. Li, Ph. D. Thesis, University of Michigan, Ann Arbor, Michigan (1989); L. Li and R. Kopelman, unpublished.
31. S. Redner, in *Extended Abstracts of Materials Research Society Symposium on Dynamics in Small Confining Systems*, J. M. Drake, J. Klafter, and R. Kopelman, eds. (1990), p. 109.
32. E. Clement, L. M. Sander, and R. Kopelman, *Phys. Rev. A* **39**:6455, 6466.
33. L. Galfi and Z. Racz, *Phys. Rev. A* **38**:3151 (1988).
34. Y. E. Koo, L. Li, and R. Kopelman, *Mol. Cryst. Liq. Cryst.* **183**:187 (1990).
35. Z. Jiang and C. Ebner, *Phys. Rev. A* **42**:7483 (1991).
36. S. Havlin, R. Kopelman, H. Taitelbaum, and G. H. Weiss, in *Extended Abstracts of Materials Research Society Symposium on Dynamics in Small Confining Systems*, J. M. Drake, J. Klafter, and R. Kopelman, eds. (1990), p. 117; S. Havlin and D. Ben-Avraham, *Adv. Phys.* **36**:695 (1987); H. Taitelbaum, S. Havlin, J. E. Kiefer, and G. H. Weiss, *J. Stat. Phys.*, this issue; H. Taitelbaum, S. Havlin, R. Kopelman, and G. H. Weiss, preprint.
37. A. J. Bard and L. R. Faulkner, *Electrochemical Methods* (Wiley, New York, 1980); Philip H. Rieger, *Electrochemistry* (Prentice-Hall, Englewood Cliffs, New Jersey, 1987).
38. H. A. Laitinen and I. M. Kolthoff, *J. Am. Chem. Soc.* **61**:3344 (1939).
39. Hans B. Jonassen, Virginia C. Chamblin, Vernon L. Wagner, Jr., and Ronald A. Henry, *Analyt. Chem.* **30**:1660 (1958).
40. H. Neurath, *Science* **93**:431 (1941).
41. H. Neurath, *Chem. Rev.* **30**:357 (1942).
42. D. L. Loughborough and A. J. Stamm, *J. Phys. Chem.* **40**:1113 (1936).
43. R. Fürth, *J. Sci. Instr.* **22**:61 (1945).
44. A. K. Attri and Allen P. Minton, *Analyt. Biochem.* **133**:142 (1983); N. Muramatsu and Allen P. Minton, *Analyt. Biochem.* **168**:345 (1988).
45. J. Topping, *Errors of Observation and their Treatment* (Chapman and Hall Ltd. and Science Paperbacks, 1971).
46. Jan F. Rabek, *Experimental Methods in Polymer Chemistry* (Wiley, New York, 1980).